Atmosphere–Ocean Interaction on Weekly Timescales in the North Atlantic and Pacific

CLARA DESER AND MICHAEL S. TIMLIN

CIRES, University of Colorado, Boulder, Boulder, Colorado

(Manuscript received 9 February 1996, in final form 15 July 1996)

ABSTRACT

Large-scale atmosphere–ocean interaction over the North Atlantic and North Pacific during winter using a 14-yr record of weekly sea surface temperature and atmospheric circulation fields is examined. Singular Value Decomposition is used to quantify objectively the degree of coupling between the sea surface temperature and 500-mb geopotential height fields as a function of time lag, from −4 weeks to +4 weeks. The authors show that the air–sea coupling is strongest when 500-mb height leads sea surface temperature by 2–3 weeks—twice as strong as the simultaneous covariability and nearly four times as large as when sea surface temperature leads 500-mb height by a few weeks. The authors believe the 2–3-week timescale may be a reflection of high-frequency stochastic forcing by the atmosphere on the ocean mixed layer, in line with the theoretical model of Frankignoul and Hasselmann. Sensible and latent energy fluxes at the sea surface are shown to be an important component of the atmospheric forcing. The close spatial and temporal correspondence between the fluxes and SST tendencies on weekly timescales is a testament to the quality of the datasets.

1. Introduction

The joint occurrence of large-scale sea surface temperature (SST) and atmospheric circulation anomalies in the extratropics on monthly and seasonal timescales is well known (cf. Namias 1959, 1963, 1965; Wallace et a1. 1990; Cayan 1992a,b; among others). To what extent the covariability of the atmosphere and upper-ocean results from a *cooperative* interaction between the two systems, as envisioned by Namias (1959, 1963, 1965), remains obscure. A better understanding of causality in midlatitude air–sea interaction is important from the standpoint of atmospheric predictability since the lifetime of thermal anomalies in the ocean mixed layer is on the order of several months to a year (Frankignoul 1985).

The influence of atmospheric circulation anomalies upon extratropical SSTs has been clearly demonstrated in numerous ocean modeling experiments, most recently those by Alexander (1992), Luksch and von Storch (1992), Miller et al. (1994), Battisti et al. (1995), and Delworth (1996). These studies have shown that anomalous turbulent heat fluxes, buoyancy-driven entrainment, and Ekman advection are the dominant processes whereby the atmosphere forces large-scale extratropical SST anomalies. In contrast, the extent to which the atmospheric circulation is sensitive to extratropical SST anomalies is unclear (see the recent review by Kushnir and Held 1996). Because of the high degree of natural or internal variability of the middle-latitude atmospheric circulation, empirical and modeling studies of the atmospheric response to extratropical SST anomalies are difficult to perform. Further, the parameters upon which such a reponse depends (e.g., the strength of baroclinic eddy activity and the configuration of the SST anomaly relative to the position of the stormtrack) have yet to be systematically investigated and understood. As a result, the sensitivity of the simulated atmosphere to extratropical SST anomalies is highly model dependent, with some models yielding a significant barotropic response (e.g., Palmer and Sun 1985; Ferranti et al. 1994; Latif and Barnett 1994; Peng et al. 1995), others exhibiting a baroclinic response (e.g., Hense et al. 1990; Held 1983; Ting 1991), and others exhibiting no significant response (e.g., Lau and Nath 1994; Delworth 1996). Recently, Barsugli (1995) has suggested that the *mutual* interaction of the extratropical ocean and atmosphere may lead to preferred spatial and temporal configurations of variability in an idealized coupled model setting.

Empirical studies of extratropical atmosphere–ocean interaction have examined the lag associations between monthly atmospheric and SST anomaly fields as a means of ascertaining cause and effect (Davis 1976; Lanzante 1984; Wallace and Jiang 1987). These studies find that large-scale air–sea coupling in middle latitudes during winter is strongest when the atmosphere leads the ocean by 1 month, nearly as strong in the contemporaneous fields, and negligible when the ocean leads the atmosphere. In other words, observational studies suggest

Corresponding author address: Dr. Clara Deser, CIRES, University of Colorado, Boulder, Campus Box 449, Boulder, CO 80309.
E-mail: cxd@cdc.noaa.gov

that the atmosphere is driving SST (see also Cayan 1992b). However, as noted by Wallace et al. (1990), the simultaneous relationships based on monthly data may contain both directions of air–sea interaction since the ocean mixed layer responds to atmospheric forcing events on a timescale of days to months, while the atmosphere should respond within a week if it is sensitive at all to extratropical SST anomalies. The purpose of this study is to revisit the issue of extratropical air–sea interaction using data with a temporal resolution finer than one month in the hope of obtaining a more definitive lag-correlation structure with regard to cause and effect. In particular, how does the strength of the air–sea coupling vary at weekly lags between zero and +1 month (atmosphere leading)? Are there any modes of covariability for which the distribution of lag-correlations is symmetric about zero lag or skewed toward negative lags, indicative of SST forcing the atmosphere? To what extent do anomalous fluxes of sensible and latent energy at the sea surface account for the SST changes within a month? The recent availability of a high quality weekly SST dataset (Reynolds and Smith 1995) allows these issues to be addressed. We note that any influence of internal oceanic processes on SST variability on decadal and longer timescales is excluded from the present analysis due to the limited length of the datasets.

We investigate large-scale atmosphere–ocean interaction during winter in the North Atlantic and North Pacific using a 14-yr record of weekly SST and atmospheric circulation fields, with emphasis upon the relative strength of the air–sea coupling as a function of time lag. The datasets and methods are described in section 2. Results are presented in section 3 and interpreted in section 4. Conclusions are given in section 5.

2. Data and methods

The datasets used in this study are weekly SST fields from Reynolds and Smith (1995), twice-daily 500-mb height and sea level pressure fields from the National Center for Atmospheric Research (NCAR) data library, and four-times daily surface sensible and latent heat fluxes from the National Centers for Environmental Prediction (NCEP) reanalysis project. The SST data are derived from a blend of remotely sensed and in situ data in which satellite retrievals are used to define the spatial character of the SST distribution and ship and buoy measurements provide ''ground truth'' values at irregularily spaced intervals. The weekly SST fields are then subjected to an optimum interpolation analysis; further details are provided by Reynolds and Smith (1995). The SST data begin in November 1981 and are updated in near real time.

The weekly SST fields are provided on a 1° latitude × 1° longitude grid, from which we formed 2° × 2° averages smoothed with a three-point binomial filter in both the zonal and meridional directions. The 500-mb height and sea level pressure fields are on a 2.5° latitude × 2.5° longitude grid, while the surface flux fields are on a Gaussian grid, roughly equivalent to 2° latitude × 2° longitude.

We examine the coupling between the atmosphere and ocean during winter, defined as the 27 weeks from mid-October to mid-April for the 14 yr 1981/82–1994/95. (At the time this study was performed, the surface flux fields were unavailable for the first and last two winters.) We formed weekly averages of the 500-mb height, sea level pressure, and sensible and latent heat flux fields centered at the midpoint of the SST weeks. Weekly anomalies were defined as departures from the sum of the first five harmonics of the annual cycle of the long-term weekly means based on the 14-winter period of record. Following the recommendation of Reynolds and Smith (1995), we subjected the weekly SST anomaly fields (and the weekly atmospheric anomaly fields) to a three-point binomial filter in time.

Our primary analysis tool is singular value decomposition (SVD), a technique designed to find covarying patterns in two different fields, for example, SST and 500-mb height. Since we are interested in the degree of coupling between the atmosphere and ocean at various time lags, SVD analysis provides a direct and objective method for assessing the strength of covariability between the two fields. SVD operates on the covariance matrix between two fields and provides pairs of spatial patterns (modes) whose temporal covariance is high. The SVD modes are ordered according to the amount of squared covariance explained. Further details on SVD analysis as applied to meteorological data may be found in Wallace et al. (1992), Bretherton et al. (1992), and Newman and Sardeshmukh (1995). As input to the SVD routine, we use anomaly fields normalized by the standard deviation at each grid point (see also Peng and Fyfe 1996). Note that the SVD analysis obtains modes that maximize the squared covariance (in this case, normalized covariance) between two fields, not modes that maximize the temporal correlation between the expansion coefficients of the patterns in the two fields, as in canonical correlation analysis. We perform SVD analysis between the 500-mb height and SST fields over the North Atlantic and North Pacific separately. For the Atlantic, we use 500-mb heights in the region (10°–80°N, 90°W–0°) and SSTs in the region (15°–60°N, 90°W–0°). For the Pacific, we use 500-mb heights in the region (20°–70°N, 150°E–120°W) and SSTs in the region (15°–60°N, 150°E–120°W). For both fields, only every other grid point is used in the SVD routine. The results are not sensitive to the precise definitions of the domains. A separate SVD analysis is carried out for each time lag between −4 weeks and +4 weeks. To lend support to the results based upon SVD analysis, we use empirical orthogonal function (EOF) analysis and a case study approach.

TABLE 1. Total temporal squared covariance between normalized SST and 500-mb height anomalies over the North Atlantic during winter as a function of lag in weeks. Negative (positive) lags indicate SST leads (lags) the atmosphere. Units are nondimensional as each grid point has been normalized by its respective standard deviation. The simultaneous covariance has been arbitrarily assigned a value of 100 units. (Top row) Unfiltered data; (bottom row) intraseasonal data.

	Lag in weeks								
	−4	−3	−2	−1	0	1	2	3	4
Unf	53	51	51	64	100	141	159	155	140
Intra	62	59	52	57	100	158	176	164	136

3. Results

a. North Atlantic

1) OCEAN–ATMOSPHERE COVARIABILITY STATISTICS

(i) Total squared covariance

Table 1 (top row) shows the total temporal squared covariance[1] between normalized SST and 500-mb height anomalies over the North Atlantic during winter as a function of lag. The total squared covariance at a particular time lag τ is defined as

$$\Sigma_j\Sigma_i\Sigma_t(\mathrm{SST}_{i,(t-\tau)}\ \mathrm{Z500}_{j,t}),$$

where i and j are spatial indexes and t is the index for time. In Table 1, negative (positive) lags indicate SST leads (lags) the atmosphere. The simultaneous squared covariance has been arbitrarily assigned a value of 100 units. The total squared covariance shows a strong asymmetry with respect to lag, with a minimum (51 units) at lags −2 and −3 weeks and a maximum (159 units) at lag +2 weeks. In an absolute sense, the mean squared covariance at lag +2 weeks is 0.039, formed by summing the squared covariances for all pairs of grid points and dividing by the number of grid points.

Since winter-to-winter fluctuations do not contribute to the asymmetry of the lag covariances, we recomputed the covariance statistics using data from which the winter means were first removed (Table 1, bottom row). We shall refer to these data as ''intraseasonal'' since only those fluctuations with timescales less than a season contribute to the variability. As expected, the asymmetry of the total squared covariance with respect to lag is even more pronounced for the intraseaonal data than for the unfiltered data, with a minimum (52 units) at lag −2 weeks and a maximum (176 units) at lag +2 weeks. In an absolute sense, the mean squared covariance at lag +2 weeks is 0.046. It is worth noting that when both the unfiltered and intraseasonal data are normalized by the standard deviations based upon the unfiltered data, the ratio of intraseasonal to total simultaneous squared covariance is 0.68.

[1] Strictly speaking, the covariance between two records that have been normalized by their respective standard deviations is the correlation. However, we retain the term ''covariance'' for conceptual ease.

TABLE 2. Singular Value Decomposition (SVD) between normalized SST and 500-mb height anomalies over the North Atlantic during winter as a function of lag in weeks. Negative (positive) lags indicate SST leads (lags) the atmosphere. Note that a separate SVD analysis was peformed for each lag. COV2 is the squared covariance accounted for by the SVD mode, R is the temporal correlation coefficient between the expansion coefficients of the SST and 500-mb height patterns of the SVD mode, and %cov is the fraction of the total squared covariance accounted for by the SVD mode. All units are nondimensional. Results are based on unfiltered data.

	Mode 1			Mode 2		
Lag	COV2	R	%cov	COV2	R	%cov
−4	21	0.60	40	12	0.48	22
−3	21	0.59	41	11	0.48	21
−2	22	0.52	43	9	0.48	18
−1	29	0.49	46	11	0.50	17
0	50	0.55	50	17	0.58	17
1	78	0.65	55	24	0.64	17
2	95	0.69	60	26	0.66	16
3	95	0.68	62	26	0.66	17
4	85	0.65	61	26	0.63	18

(ii) Singular value decomposition of the total squared covariance

The covariability between the SST and 500-mb height fields can be decomposed into dominant patterns or ''modes'' using the technique of Singular Value Decomposition, as described in section 2. Table 2 shows the SVD results for SST and 500-mb height anomalies over the North Atlantic during winter for lags −4 to +4 weeks, based on unfiltered data. Note that a separate SVD analysis was performed for each lag. Only the first two SVD modes are shown since together they explain about two-thirds of the total squared covariance. Three statistics are shown for each mode; the squared covariance accounted for by the SVD mode, the temporal correlation coefficient between the expansion coefficients (time series) of the SST and 500-mb height patterns of the SVD mode, and the fraction of the total squared covariance accounted for by the SVD mode. Previous studies (i.e., Wallace et al. 1992; Bretherton et al. 1992) have emphasized the fractional squared covariance as a measure of the importance of a particular SVD mode. However, in the present study, we are interested in how the *actual* squared covariance of a particular SVD mode depends upon the lag between the SST and 500-mb height field: the fractional squared covariance is less sensitive to lag because both the actual and the total squared covariance vary in a similar fashion.

The first SVD mode explains 40%–62% of the total squared covariance, while mode 2 explains 16%–22%, depending on lag. The *actual* squared covariance associated with the first SVD mode varies from a minimum of 21 units at lags −3 and −4 to a maximum of

TABLE 3. As in Table 2 but for intraseasonal data.

	Mode 1			Mode 2		
Lag	COV2	R	%cov	COV2	R	%cov
−4	39	0.55	63	5	0.44	8
−3	35	0.59	60	6	0.40	10
−2	30	0.57	57	6	0.46	11
−1	34	0.52	60	8	0.42	14
0	63	0.59	63	15	0.55	15
1	106	0.70	67	21	0.64	13
2	129	0.75	73	18	0.59	10
3	128	0.73	78	14	0.56	8
4	108	0.68	79	11	0.53	8

95 units at lags +2 and +3, an increase of 450% (Table 2). The squared covariance nearly doubles between lag 0 and lag +2. A similar asymmetry with respect to lag is seen for mode 2 (Table 2) and mode 3 (not shown). The ordering of the modes is the same across all lags.

Table 3 shows the SVD results based on intraseasonal data. Mode 1 of the intraseasonal data explains 57%–79% of the total squared covariance, while mode 2 explains 8%–15%, depending on lag. The actual squared covariance associated with mode 1 ranges from a minimum of 30 units at lag −2 weeks to a maximum of 129 units at lag +2 weeks, an increase of a factor of 4.3. (Note that the squared covariance values in Tables 2 and 3 cannot be directly compared since both are normalized by different total squared covariances at lag 0.)

In summary, the covariability between SST and 500-mb height anomalies over the North Atlantic during winter exhibits a distinct asymmetry with respect to lag, both in the total fields (Table 1) and in the SVD decompositions (Tables 2 and 3), with minimum covariability when SST leads the 500-mb height field by 2 weeks and maximum covariability when SST lags the atmosphere by 2–3 weeks. The covariability increases approximately four-fold from lag −2 to lag +2 weeks and doubles from lag 0 to lag +2 weeks.

2) SPATIAL PATTERNS OF OCEAN–ATMOSPHERE COVARIABILITY

(i) SVD between 500-mb height and SST

Figures 1a–c show the spatial patterns of normalized 500-mb height (top) and SST (bottom) anomalies for the leading intraseasonal SVD mode at lag −2, 0, and +2 weeks, respectively (the corresponding patterns based on unfiltered data are similar; not shown). Each pair of patterns was formed from the so-called heterogeneous correlations (see Wallace et al. 1992); for example, the expansion coefficient of the SST SVD pattern was correlated with the time series of 500-mb height anomalies at each grid point to form the normalized 500-mb height anomaly pattern, and the expansion coefficient of the 500-mb height SVD pattern was correlated with the time series of SST anomalies at each grid point to form the normalized SST anomaly pattern. The progressive organization and strengthening of the coupled 500-mb height and SST anomaly patterns from lag −2 weeks (Fig. 1a) to lag +2 weeks (Fig. 1c) is evident, consistent with the statistics presented in Table 2. Maximum correlation coefficients are ~0.7 in absolute value for the strongest coupled patterns (Fig. 1c). The 500-mb height field consists of a north–south-oriented dipole with centers over southern Greenland and along 35°N in the central Atlantic and a center over western Russia reminiscent of the west Atlantic pattern defined by Wallace and Gutzler (1981). The SST pattern is organized into zonal bands of alternating polarity, with an additional center over the Norwegian and Baltic Seas. These structures are similar to those obtained in numerous previous studies based on monthly and seasonal data using a variety of analysis techniques, including Cayan (1992a,b) and Kushnir (1994; his Fig. 13).

The time series or expansion coefficients of the 500-mb height and SST anomaly patterns of the leading SVD mode at lag +2 weeks are shown in Fig. 2a for the unfiltered data and in Fig. 2b for the intraseasonal data. Each winter is represented by a continuous curve with gaps between winters. The 2–3-week lag between 500-mb height and SST is visually apparent in both the unfiltered and intraseasonal records, even for the lower-amplitude fluctuations of the last four winters. The correlation coefficient between the two curves is 0.69 for the unfiltered data and 0.75 for the intraseasonal records at a lag of +2 weeks (see Tables 2 and 3).

The sequence of SVD analyses presented in Figs. 1a–c may not neccesarily represent a temporal progression of 500-mb height and SST anomaly patterns, unless the expansion coefficients of the modes are all highly correlated when lagged appropriately. It turns out that the 500-mb expansion coefficients *are* nearly identical except for a phase lag, so that the SST patterns in Fig. 1 may be viewed as a temporal sequence. This is not the case, however, for the SST expansion cofficients. To show the temporal evolution of the 500-mb height field associated with the SST pattern in Fig. 1c, we correlated the 500-mb height data with the lag +2 SVD SST expansion coefficient at lag −2, 0, and +2 weeks (Fig. 3). Relative to the SST field, the 500-mb height correlations attain their maximum strength two weeks before and decay to near zero 2 weeks after. Note the difference between the bottom panel of Fig. 3 and the lag −2 SVD mode (Fig. 1a).

To help confirm the SVD results, we performed EOF analysis upon the normalized SST anomaly field. The spatial pattern of the leading EOF (not shown) is nearly indistinguishable from its SST counterpart based on SVD analysis with the 500-mb height field. The maximum lag correlation between the expansion coefficient of the leading EOF of SST and that of the leading SST pattern derived from SVD analysis with the 500-mb

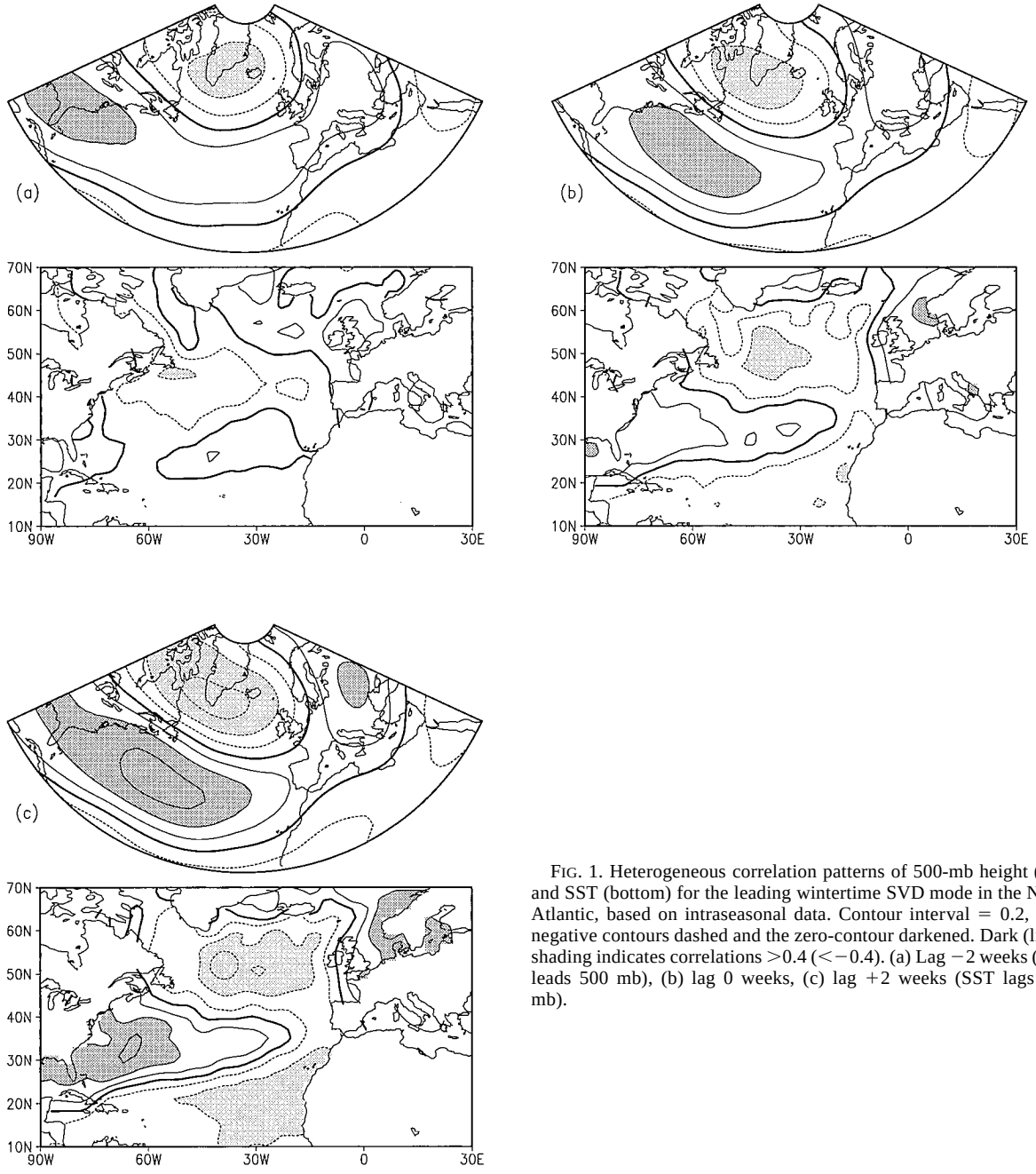

FIG. 1. Heterogeneous correlation patterns of 500-mb height (top) and SST (bottom) for the leading wintertime SVD mode in the North Atlantic, based on intraseasonal data. Contour interval = 0.2, with negative contours dashed and the zero-contour darkened. Dark (light) shading indicates correlations >0.4 (<-0.4). (a) Lag -2 weeks (SST leads 500 mb), (b) lag 0 weeks, (c) lag $+2$ weeks (SST lags 500 mb).

height field at lag $+2$ is 0.96. Correlating the expansion coefficient of the SST EOF with the 500-mb height field at lags -2, 0, and $+2$ weeks yields patterns very similar to those in Fig. 3 based upon SVD analysis (not shown).

To further verify the result that large-scale air–sea coupling in the North Atlantic is stronger when the atmosphere leads SST by several weeks than in the contemporaneous fields, we have examined numerous case studies. An example is shown in Fig. 4, which depicts the normalized 500-mb height and SST anomalies for the second week in December 1989 (left) and 3 weeks later, the first week of January 1990 (right). A strong atmospheric circulation anomaly pattern is evident in the second week of December 1989, with above normal heights over Greenland and below normal heights along $\sim 40°$N in the Atlantic. Three weeks later, the anomalous circulation over the Atlantic has weakened considerably as the high shifts eastward into Scandinavia. In contrast, the SST anomaly pattern strengthens during the 3-week period, particularly south of 50°N. Thus, by the first week of January 1990, the basinwide SST field is

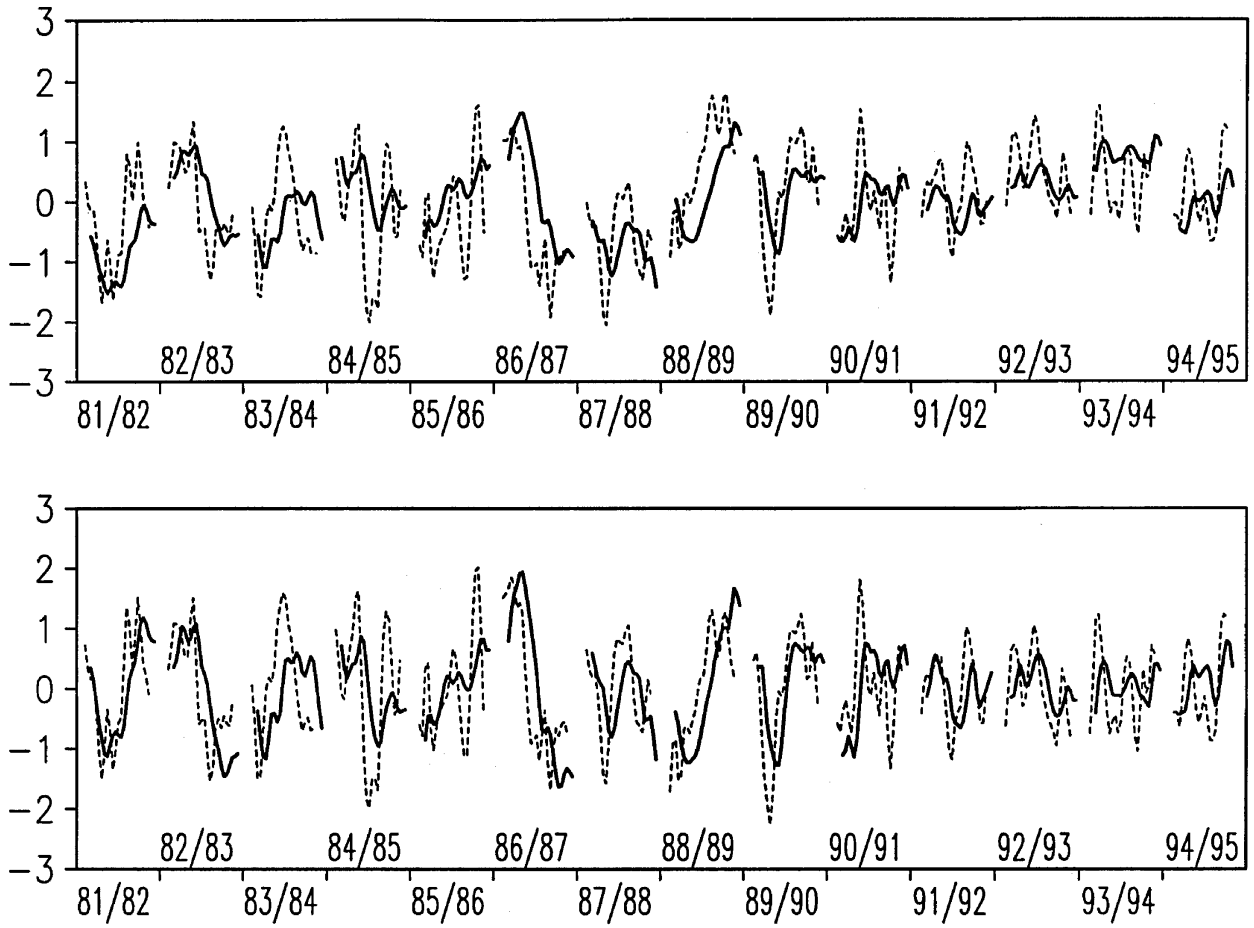

FIG. 2. Expansion coefficients (time series) of the leading Atlantic wintertime SVD mode between 500-mb height (dashed) and SST (solid) at lag +2 weeks. Data are shown for each winter as indicated, with gaps between winters: (top) unfiltered, (bottom) intraseasonal. The correlation coefficient is 0.69 for the unfiltered records and 0.75 for the intraseasonal records at lag +2 weeks.

strongly anomalous, while the overlying atmospheric circulation is relatively normal.

(ii) SVD between the atmosphere and SST tendency field

One can exploit the natural asymmetry in the lag statistics presented in Tables 1–3 by performing SVD analysis upon the 500-mb height field and the SST *tendency* field, defined as the change in SST from week −2 to week +2 relative to the 500-mb height field. The SST tendency field is directly related to atmospheric forcing through the heat budget equation for the ocean mixed layer, as discussed in section 4. The spatial pattern of the first SVD mode between 500-mb heights and SST tendencies over the North Atlantic during winter is shown in Fig. 5 (mode 1 accounts for 70% of the total squared covariance, with the second mode explaining 12%). The 500-mb height data were subjected to a 3-week running mean, centered at the midpoint of the SST tendency. Both the SST tendency and 500-mb height patterns are similar in structure to those based on the lag +2 SVD calculation between SST and 500 mb. The negative SST tendency anomaly in the subpolar North Atlantic is located ~15° of longitude farther east than its counterpart in Fig. 1c, consistent with the eastward expansion of the subpolar SST anomalies from lag 0 to lag +2 in the SVD analyses. The time series of the 500-mb height and SST tendency patterns are shown in the bottom panel of Fig. 5. The correlation coefficient between the two records is 0.79.

The physical relationship between the atmospheric circulation and SST fields may be more readily interpreted by comparing the unnormalized anomaly patterns of sea level pressure (SLP) and SST tendency. Figure 6 shows the regression patterns of SLP and SST tendency based on the time series of the SST tendency pattern derived from SVD between 500-mb height and SST tendency. The regression fields give the typical anomaly patterns associated with a unit departure of the SST tendency time series. It is evident that each of the SST tendency anomaly centers corresponds to a region of large SLP gradient or geostrophic wind anomaly. For example, the negative SST tendency center between

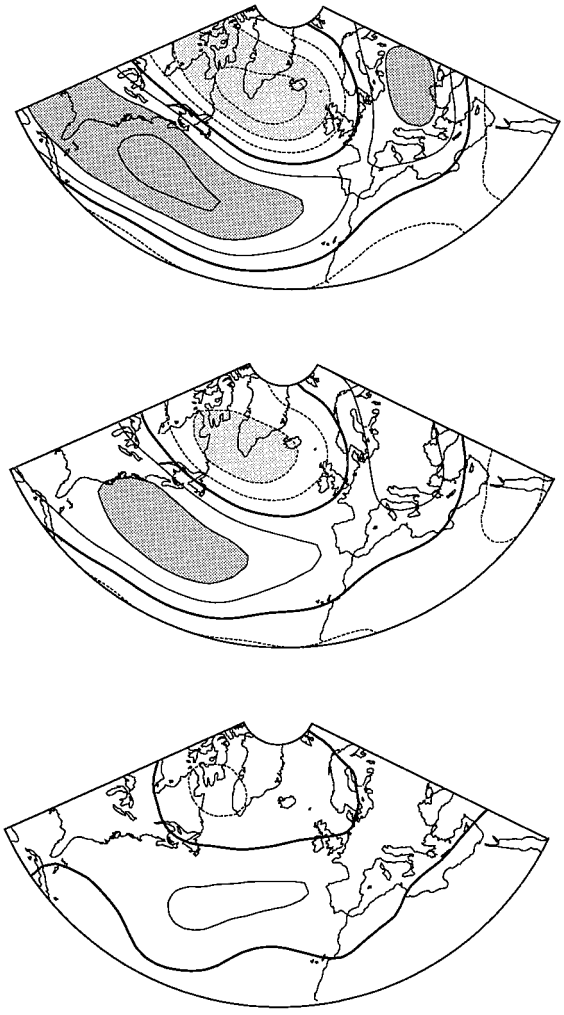

FIG. 3. The 500-mb height correlations with the lag +2 SST SVD expansion coefficient, based on intraseasonal data: (top) 500-mb heights leading SST by 2 weeks, (middle) simultaneous, and (bottom) 500-mb heights lagging SST by 2 weeks. Contour interval = 0.2, with negative contours dashed and the zero contour darkened. Dark (light) shading indicates correlations >0.4 (<−0.4).

Newfoundland and Ireland is associated with stronger than normal surface westerly northwesterly winds. These wind anomalies can cool the ocean mixed layer via increased evaporation and sensible heat loss, as well as by enhanced entrainment of cooler water from beneath the mixed layer (c.f. Battisti et al. 1995). Analagous arguments can be made for the other SST tendency centers in Fig. 6.

To verify the notion that surface fluxes may be instrumental in creating the SST tendency anomalies, we performed SVD analysis upon the sum of the sensible and latent heat fluxes from the NMC reanalysis dataset and the SST tendency field. Previous studies (cf. Cayan 1992a; Battisti et al. 1995) have shown that the turbulent fluxes dominate the net surface energy flux over the extratropical oceans during winter. The first SVD mode, shown in Fig. 7, explains 65% of the total covariance squared and exhibits a 0.87 correlation coefficient between the expansion coefficients of the flux and SST tendency patterns. As expected, the anomalous fluxes of sensible and latent heat are collocated with the anomalous SST tendency centers, with areas of enhanced energy flux out of (into) the ocean corresponding to regions of decreasing (increasing) SST. While the notion that turbulent energy fluxes play a dominant role in creating large-scale extratropical SST anomaly patterns in winter is well known, the close spatial and temporal correspondence between the fluxes and SST tendencies on weekly timescales has not been demonstrated previously and is a testament to the quality of the datasets.

We compare the magnitudes of the observed SST tendencies and those induced by the surface turbulent energy fluxes in Fig. 8. The observed SST tendencies were obtained by regressing the tendency fields upon the expansion coefficient of the leading SVD pattern of SST tendency shown in Fig. 7. Similarily, the flux-induced SST tendencies were formed by regressing the sum of the latent and sensible heat flux anomalies upon the SST tendency expansion coefficient, and scaling them by the factor (ρ Cp H), where ρ is the density of water, Cp the heat capacity of water, and H is the observed climatological mean mixed layer depth for November–March, given by Levitus (1982). (The mixed layer depths are provided on a monthly $1^\circ \times 1^\circ$ grid: to form the predicted SST tendencies, we interpolated both the mixed layer depth and surface flux data onto a $2^\circ \times 2^\circ$ grid.) Both the observed and predicted SST tendencies have units of degrees Celcius per day per unit departure of the SST tendency expansion coefficient. Figure 8 shows there is good agreement between the magnitudes of the large-scale observed SST tendencies and those induced by the latent and sensible heat fluxes over most of the North Atlantic. (The predicted SST tendencies along the coast of Greenland and in the Labrador Sea occur in regions of high sea ice concentration and as such are probably spurious.) For the North Atlantic as a whole, the ratio of the observed to surface flux-induced SST tendency anomalies is 1.3, as given by the sum of the absolute value of the SST tendency at each oceanic grid point, excluding the coast of Greenland and the Labrador Sea.

In the western Atlantic, the largest flux-induced SST tendencies occur along the southeastern seaboard of the United States, while the largest observed SST tendencies are found farther north and east. One plausible explanation for the displacement between the flux-induced and observed SST tendencies is advection by the Gulf Stream. We note that for an average surface velocity of 1 m s^{-1} (Stommel 1965) the Gulf Stream could advect the heat input to the ocean mixed layer a distance of ~1500 km (e.g., from Cape Hatteras to south of Nova Scotia) in 2.5 weeks. Thus, the actual change in SST during a 4-week period may occur substantially downstream of where the heat is put in by the atmosphere.

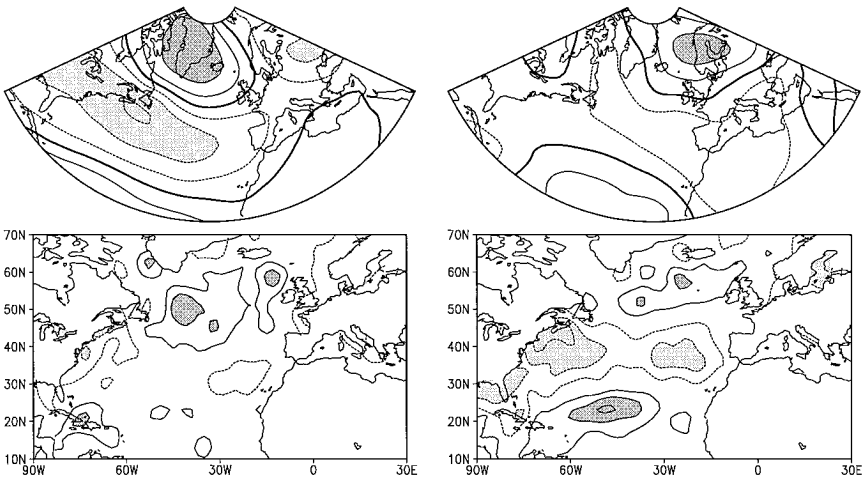

FIG. 4. Normalized 500-mb height (top) and SST (bottom) anomalies for the second week of December 1989 (left) and 3 weeks later (right). Contour interval = 1 standard deviation, with negative contours dashed and the zero contour darkened. Dark (light) shading indicates values >2 (<-2) standard deviations. The zero contours in the SST fields have been omitted for clarity.

b. North Pacific

1) OCEAN–ATMOSPHERE COVARIABILITY STATISTICS

(i) Total squared covariance

Table 4 (top row) shows the total squared covariance between 500-mb heights and SSTs in the North Pacific as a function of lag. The total squared covariance reaches a minimum at lag -3 weeks (57 units) and a maximum at lag $+3$ weeks (151 units). For the intraseasonal data (Table 4, bottom row), the asymmetry of the total squared covariance with respect to lag is more clearly defined, with a minimum at lag -1 week (57 units) and a maximum at lag $+2$ weeks (202 units). These values are similar to those for the Atlantic (Table 1).

(ii) Singular value decomposition of the total squared covariance

Table 5 shows the results of SVD analysis between 500-mb heights and SSTs over the North Pacific based on unfiltered data. The first SVD mode accounts for 43%–55% of the total squared covariance depending on lag, approximately twice as much as the second mode. The ordering of the modes is the same across all lags. The squared covariance associated with mode 1 (mode 2) increases by a factor of 3.1 (2.7) from a minimum at lag -3 weeks to a maximum at lag $+3$ weeks: somewhat less than for the first mode in the Atlantic (4.5), reflecting the larger proportion of interannual variability in the Pacific during 1982–95. The ENSO phenomenon in the tropical Pacific, with its known teleconnections to the North Pacific (e.g., Hoskins and Karoly 1981), may be one source of the enhanced interannual variability over the North Pacific compared to the North Atlantic.

When SVD analysis is applied to the intraseasonal data, the order of the two leading modes is reversed from their unfiltered counterparts. The temporal correlation coefficient between intraseasonal mode 2 and the intraseasonal component of unfiltered mode 1 is 0.9 for the Z500 expansion coefficients and 0.8 for the SST expansion coefficients for the lag $+2$ SVD. Nearly identical correlation coefficients are found for intraseasonal mode 1 and the intraseasonal component of unfiltered mode 2. Table 6 shows the SVD results for the intraseasonal data. The squared covariances associated with the two leading intraseasonal modes exhibit a strong asymmetry with respect to lag, with a minimum at lag -2 weeks and a maximum at lag $+2$ weeks. The covariability increases by nearly a factor of 5 from lag -2 to lag $+2$ weeks and doubles from lag 0 to lag $+2$ weeks for both modes. Mode 1 explains approximately 50% more variance than mode 2.

2) SPATIAL PATTERNS OF OCEAN–ATMOSPHERE COVARIABILITY

(i) SVD between 500-mb height and SST

Figures 9a–c show the spatial patterns of normalized 500-mb height (top) and SST (bottom) anomalies for the leading intraseasonal SVD mode at lag -2, 0, and $+2$ weeks, respectively. Figures 10a–c show the corresponding results for the second SVD mode. Both modes show a progressive organization and strengthening of the coupled patterns from lag -2 weeks (Figs. 9a and 10a) to lag $+2$ weeks (Figs. 9c and 10c), consistent with the statistics presented in Table 6. The strongest coupled patterns (lag $+2$ weeks) of mode 1 consist of 500-mb height anomalies along 35°N with anomalies of the opposite sign over eastern Siberia extending southward along the west coast of North America, and SST anomalies in the central and western North

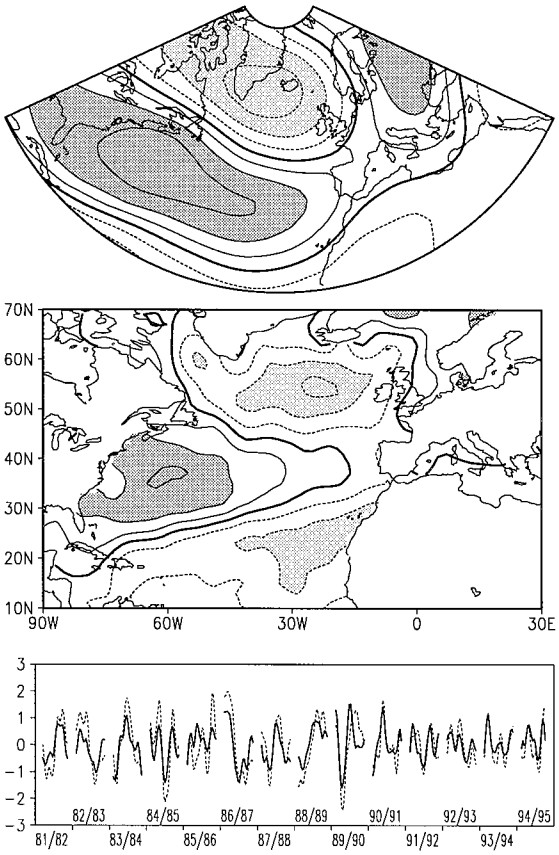

FIG. 5. Heterogeneous correlation patterns for the leading Atlantic wintertime SVD mode between 500-mb height (top) and SST tendency (middle; defined as the change in SST from week −2 to week +2 relative to the 500-mb height record). Contour interval = 0.2, with negative contours dashed and the zero contour darkened. Dark (light) shading indicates correlations >0.4 (<−0.4). This mode explains 70% of the coupled variability between the two fields. The expansion coefficients (time series) of the two patterns (bottom) are correlated at 0.79.

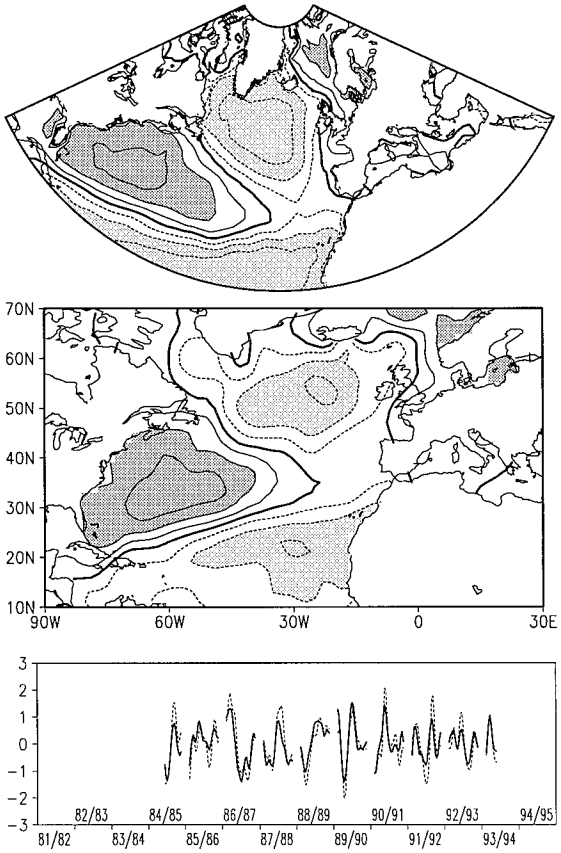

FIG. 7. Heterogeneous correlation patterns for the leading Atlantic wintertime SVD mode between the sum of the latent and sensible heat fluxes (positive downward; top) and SST tendency (middle; defined as the change in SST from week −2 to week +2 relative to the heat flux record). Contour interval = 0.2, with negative contours dashed and the zero contour darkened. Dark (light) shading indicates correlations >0.4 (<−0.4). This mode explains 65% of the coupled variability between the two fields. The expansion coefficients (time series) of the two patterns (bottom) are correlated at 0.87.

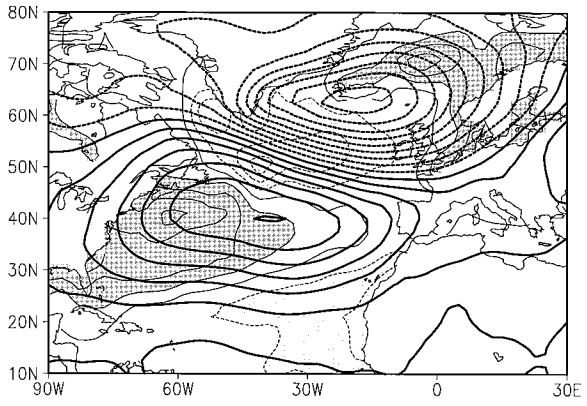

FIG. 6. Regression coefficients of sea level pressure (contours) and SST tendency (shaded) upon the SST tendency time series derived from SVD analysis with the 500-mb height field. Positive (negative) SLP anomalies are solid (dashed), and positive (negative) SST tendency anomalies are indicated by dark (light) shading.

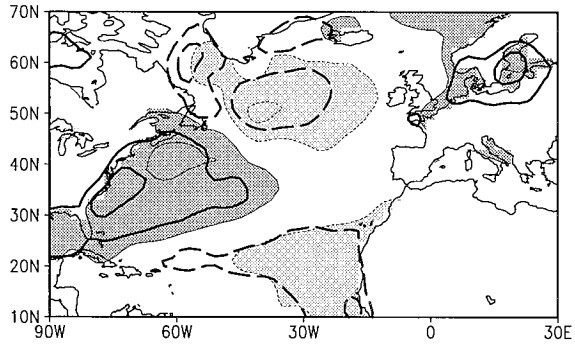

FIG. 8. Observed (shading and thin contours) and heat-flux induced (thick contours) SST tendencies associated with the leading SVD mode in the Atlantic. Units are °C day^{-1} per unit departure of the SST tendency expansion coefficient. Positive (negative) SST tendency anomalies are indicated by dark shading and solid contours (light shading and dashed contours). Contour levels are −6, −2, 2, and 6.

TABLE 4. Total temporal squared covariance between normalized SST and 500-mb height anomalies over the North Pacific during winter as a function of lag in weeks. Negative (positive) lags indicate SST leads (lags) the atmosphere. Units are nondimensional. The simultaneous covariance has been arbitrarily assigned a value of 100 units. (Top row) Unfiltered data; (bottom row) intraseasonal data.

	Lag in weeks								
	−4	−3	−2	−1	0	1	2	3	4
Unf	58	57	58	71	100	134	150	151	145
Intra	81	74	61	57	100	173	202	186	154

Pacific along ~30°N with anomalies of the opposite sign in the eastern North Pacific. The strongest coupled patterns of mode 2 include a 500-mb height distribution that resembles the Pacific–North American teleconnection pattern (Wallace and Gutzler 1981) and an SST distribution similar to the first mode but shifted 5°–10° farther north. Both patterns have been documented extensively in the literature (cf. Wallace et al. 1990; Cayan 1992; Deser and Blackmon 1995).

The temporal evolution of the 500-mb height field associated with the SST patterns in Figs. 9c and 10c are shown in Figs. 11 and 12, respectively. As in the Atlantic, the 500-mb height correlations peak two weeks before the SST pattern reaches its maximum amplitude and weaken dramatically 2 weeks after.

To help confirm the SVD results, we performed EOF analysis upon the normalized SST anomaly field. As in the Atlantic, the spatial patterns of the two leading EOFs are nearly indistinguishable from their counterparts based on SVD analysis (not shown).

(ii) SVD between 500-mb heights and the SST tendency field

The two leading SVD modes between 500-mb height and SST tendency are shown in Figs. 13 and 14, respectively. The first (second) mode explains 49% (32%) of the total squared covariance and exhibits a correlation of 0.80 (0.77) between the two expansion coefficients. The patterns are very similar to those between 500-mb height and SST based on intraseasonal data (recall Figs. 9c and 10c).

The role of surface turbulent energy fluxes in generating the SST tendency patterns shown above is examined next by comparing the magnitudes of the observed SST tendencies with those induced by the sensible and latent heat fluxes. Figure 15 (top) shows the observed and flux-induced SST tendencies associated with mode 1, obtained by regressing the SST tendency field, and the sum of the latent and sensible heat flux anomalies scaled by (ρ Cp H) upon the expansion coefficient of the leading SVD mode between 500-mb height and SST tendency. Figure 15 (bottom) shows analagous results for the second mode. Note that climatological mean mixed layer depths for November–March from Levitus (1982) were used to estimate H.

TABLE 5. Singular Value Decomposition (SVD) between normalized SST and 500-mb height anomalies over the North Pacific during winter as a function of lag in weeks. Negative (positive) lags indicate SST leads (lags) the atmosphere. Note that a separate SVD analysis was performed for each lag. COV2 is the squared covariance accounted for by the SVD mode, R is the temporal correlation coefficient between the expansion coefficients of the SST and 500-mb height patterns of the SVD mode, and %cov is the fraction of the total squared covariance accounted for by the SVD mode. All units are nondimensional. Results are based on unfiltered data.

	Mode 1			Mode 2		
Lag	COV2	R	%cov	COV2	R	%cov
−4	25	0.46	43	14	0.60	23
−3	26	0.44	46	14	0.59	25
−2	28	0.44	49	15	0.63	26
−1	37	0.48	52	17	0.65	24
0	51	0.56	51	20	0.61	20
1	67	0.63	50	31	0.59	23
2	76	0.67	51	38	0.65	26
3	81	0.68	53	38	0.62	25
4	81	0.67	55	35	0.59	24

Figure 15 shows that for both SVD modes there is good agreement between the magnitudes of the large-scale observed SST tendencies and those induced by the latent and sensible heat fluxes over much of the North Pacific. The ratio of the observed to surface flux-induced SST tendency anomalies for the North Pacific as a whole is 1.2 for mode 1 and 1.3 for mode 2, as given by the sum of the absolute value of the SST tendency at each oceanic grid point in the region (12°–60°N, 152°E–100°W).

4. Discussion

The main result of this study is that atmosphere–ocean coupling over the North Atlantic and Pacific during winter is strongest when the atmosphere leads SST by 2–3 weeks, twice as strong as the simultaneous covariability and nearly four times as large as when SST leads the atmosphere by a few weeks. Previous large-scale air–sea interaction studies were based on monthly data (cf. Davis 1976; Wallace and Jiang 1987): these studies found that the atmosphere–ocean coupling is comparable at zero lag and when the atmosphere leads SST by 1 month (and negligible when SST leads the at-

TABLE 6. As in Table 5 but for intraseasonal data.

	Mode 1			Mode 2		
Lag	COV2	R	%cov	COV2	R	%cov
−4	39	0.52	49	20	0.43	25
−3	31	0.49	42	19	0.43	26
−2	21	0.47	35	13	0.46	22
−1	19	0.48	32	14	0.41	25
0	38	0.48	38	29	0.50	29
1	76	0.63	44	53	0.60	31
2	97	0.70	48	65	0.65	32
3	95	0.68	51	62	0.63	33
4	82	0.64	53	50	0.57	33

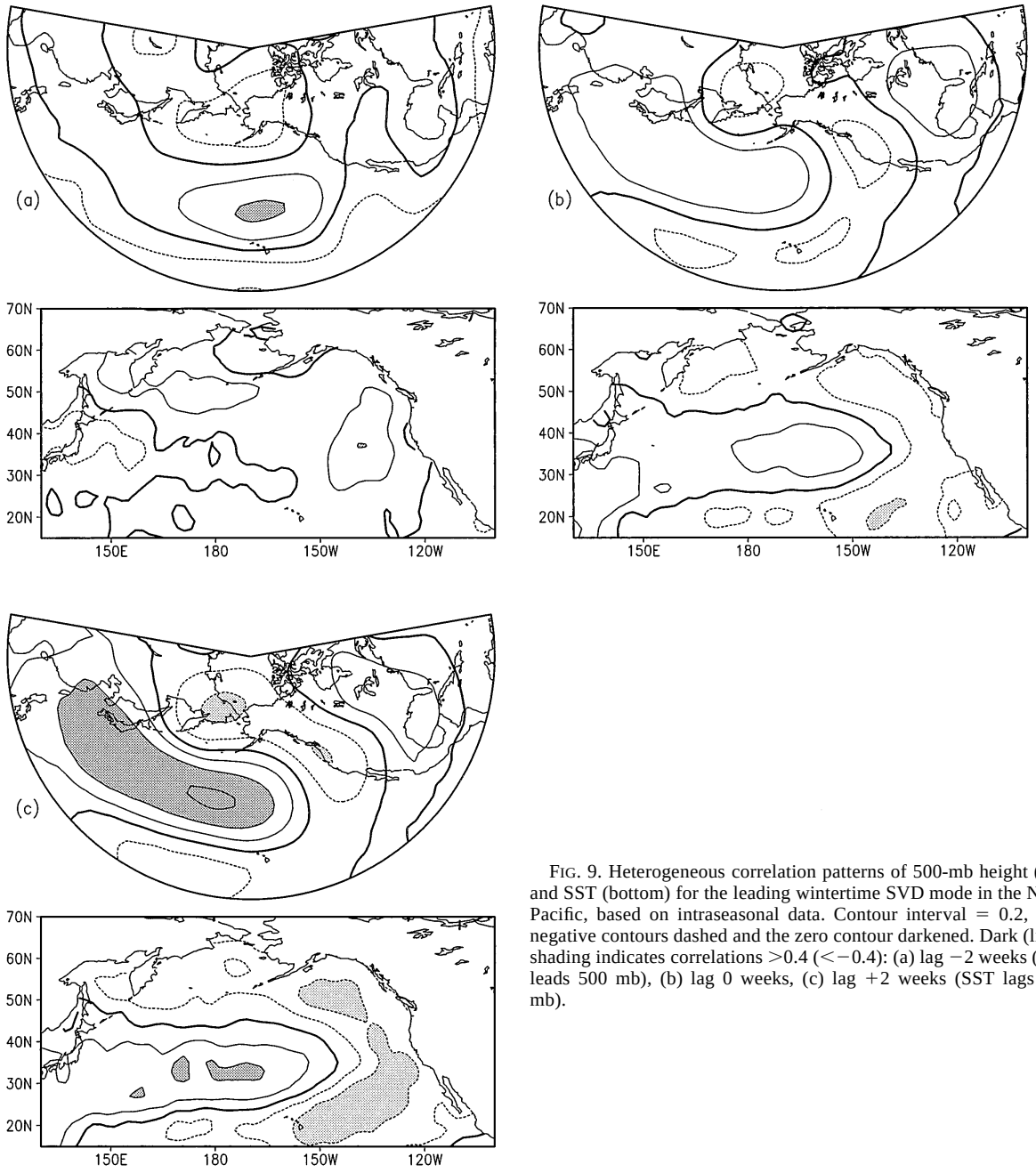

FIG. 9. Heterogeneous correlation patterns of 500-mb height (top) and SST (bottom) for the leading wintertime SVD mode in the North Pacific, based on intraseasonal data. Contour interval = 0.2, with negative contours dashed and the zero contour darkened. Dark (light) shading indicates correlations >0.4 (<-0.4): (a) lag -2 weeks (SST leads 500 mb), (b) lag 0 weeks, (c) lag $+2$ weeks (SST lags 500 mb).

mosphere by 1 month). Thus, the use of weekly data has resulted in a more sharply defined structure of the lead–lag relationships between the extratropical atmospheric circulation and SST fields. A practical lesson to be learned from the results is that SST anomalies forced by atmospheric circulation anomalies should be expected to reach their peak several weeks after the maximum atmospheric forcing.

We interpret the results within the framework of the stochastic atmospheric forcing model developed by Frankignoul and Hasselmann (1977) based on earlier work by Hasselmann (1976). According to Frankignoul and Hasselmann (1977), ''the basic premise of the stochastic forcing model is that SST anomalies represent the integral response to short-time scale atmospheric forcing.'' An underlying assumption of the model is that the characteristic timescale of the atmospheric forcing is much smaller than that of the SST response. The basic equation of the stochastic forcing model is

$$(\rho\, C_p\, H)\, dT/dt = Q(t) - \lambda T,$$

where ρ is the density of sea water, C_p is the heat ca-

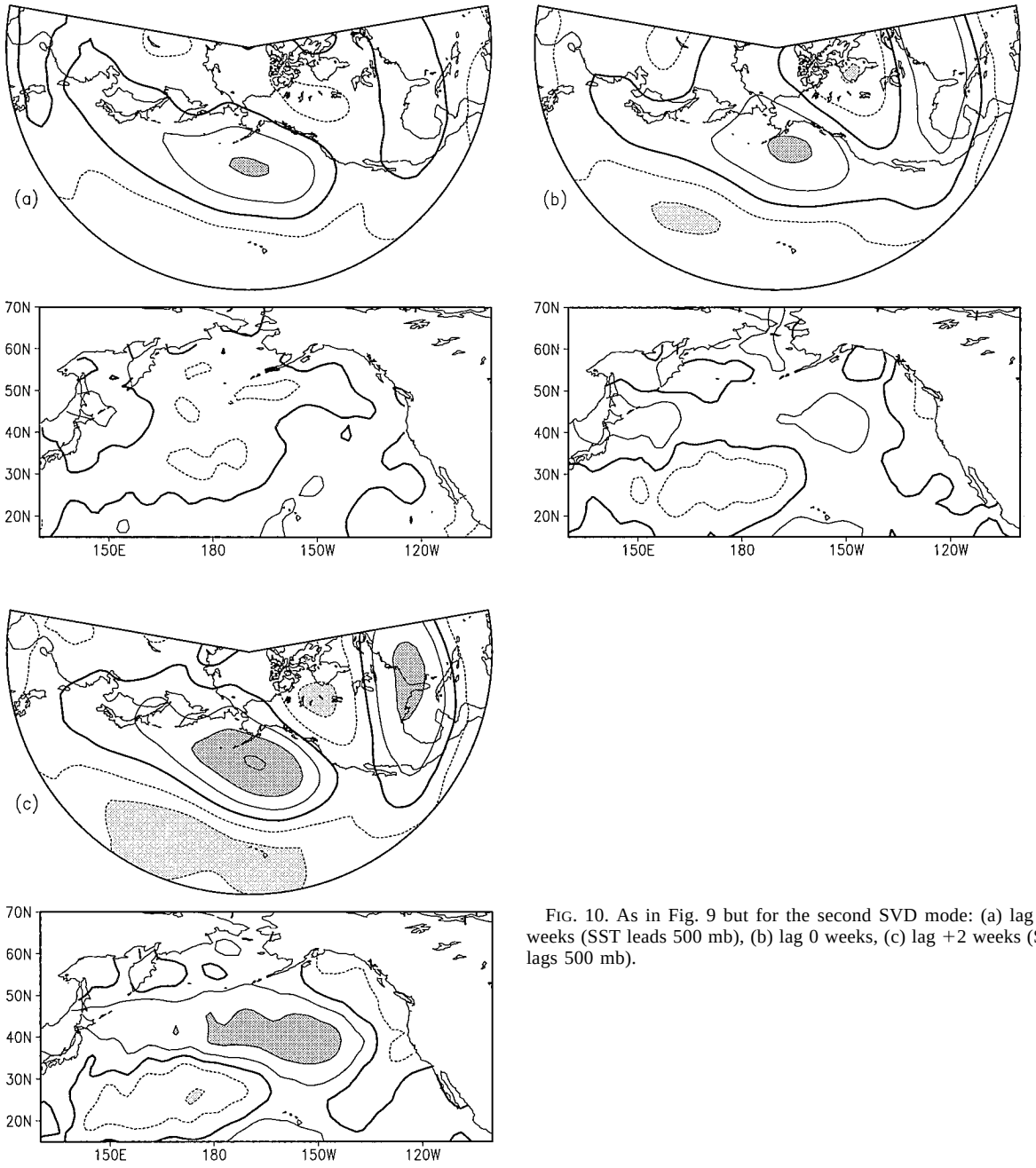

FIG. 10. As in Fig. 9 but for the second SVD mode: (a) lag −2 weeks (SST leads 500 mb), (b) lag 0 weeks, (c) lag +2 weeks (SST lags 500 mb).

pacity of water, H is the ocean mixed layer depth, T is SST, t is time, Q is the atmospheric forcing [with a characteristic timescale of $\sim$(4–10 days)$^{-1}$], and $[\lambda/(\rho C_p H)]^{-1}$ is the relaxation time of the ocean mixed layer, on the order of (4–8 months)$^{-1}$. Physically, λ represents the rate of damping of the SST anomaly through upward radiative and turbulent energy fluxes. Frankignoul and Hasselmann (1977), Reynolds (1978), Frankignoul and Reynolds (1983), and Frankignoul (1985) present numerous observations supporting the range of characteristic timescales for the atmospheric forcing and ocean mixed layer given above. We have verified that these timescales are appropriate for the patterns of extratropical atmosphere–ocean interaction found in this study (not shown). An analytical expression for the lag cross correlation function between Q and T, which depends on only the two characteristic timescales, may be derived as shown in the appendix of Frankignoul and Hasselmann (1977).

Figure 16 shows the theoretical lag cross correlation curve between Q and T according to the stochastic forcing model, using an e-folding timescale of (8 days)$^{-1}$

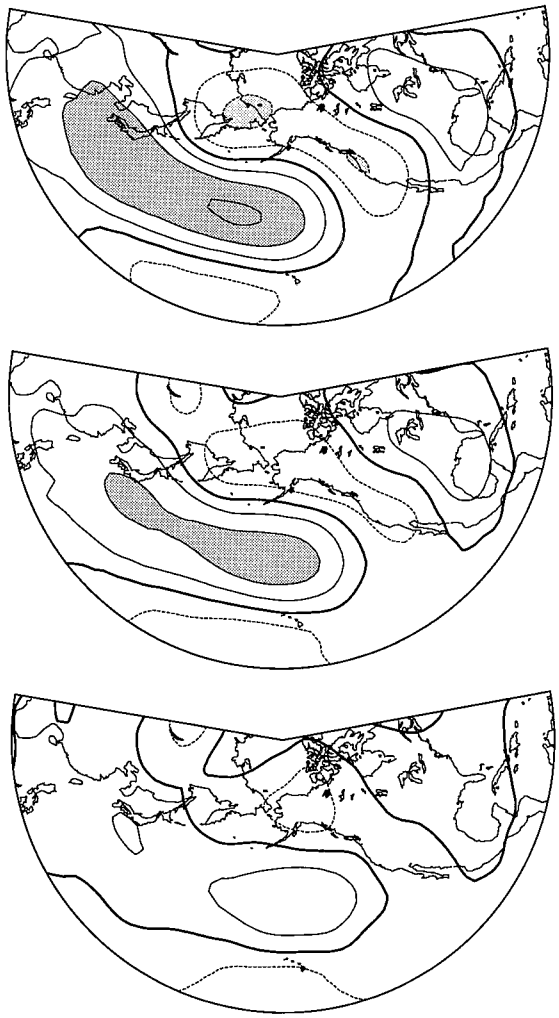

FIG. 11. The 500-mb height correlations with the lag +2 SST SVD mode 1 expansion coefficient, based on intraseasonal data. (Top) 500-mb heights leading the SST expansion coefficient by 2 weeks, (middle) simultaneous, and (bottom) 500-mb heights lagging the SST expansion coefficient by 2 weeks. Contour interval = 0.2, with negative contours dashed and the zero contour darkened. Dark (light) shading indicates correlations >0.4 (<-0.4).

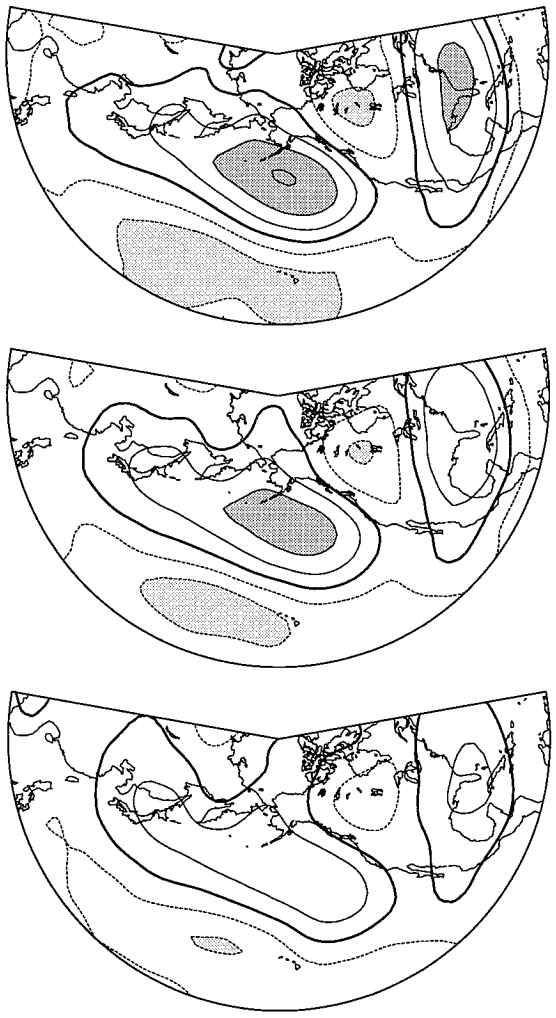

FIG. 12. As in Fig. 11 but for SVD mode 2.

for the atmospheric forcing and (5 months)$^{-1}$ for the ocean mixed layer temperature anomalies. The maximum cross correlation occurs at a lag of 18 days. The time lags of the maximum cross correlation for other reasonable choices of *e*-folding timescales are given in Table 7: all fall within the range of 11–22 days. Thus, the observed time lags (2–3 weeks) fit well with those predicted by the simple theoretical stochastic forcing model. In physical terms, one may consider the following scenario: a given atmospheric forcing pattern lasts for a week or two, during which time the SST anomaly grows; then, as the atmospheric forcing diminishes, the SST damping term outweighs the forcing and the SST anomaly begins to decay. Thus, the maximum SST anomaly is reached sometime after the peak of the atmospheric forcing.

With regard to the SST tendency results, two studies are of particular relevance: Cayan (1992b) and Wallace et al. (1990). Cayan (1992b) performed canonical correlation analysis on the SST tendency and surface turbulent heat flux fields over the North Atlantic and North Pacific to find the coupled patterns of variability. He used the change in SST from December to February to estimate the SST tendency and heat fluxes averaged from December to February. Cayan (1992) showed that seasonal anomalies of surface heat flux and SST tendency are well correlated in space and time, in keeping with the results of this study. A quantitative comparison of the observed and surface flux-induced SST tendencies was given for selected regions only.

Wallace et al. (1990) also examined the SST tendency field in relation to 500-mb height anomalies over the Northern Hemisphere oceans, using the change in SST from early winter (October–December) to late winter

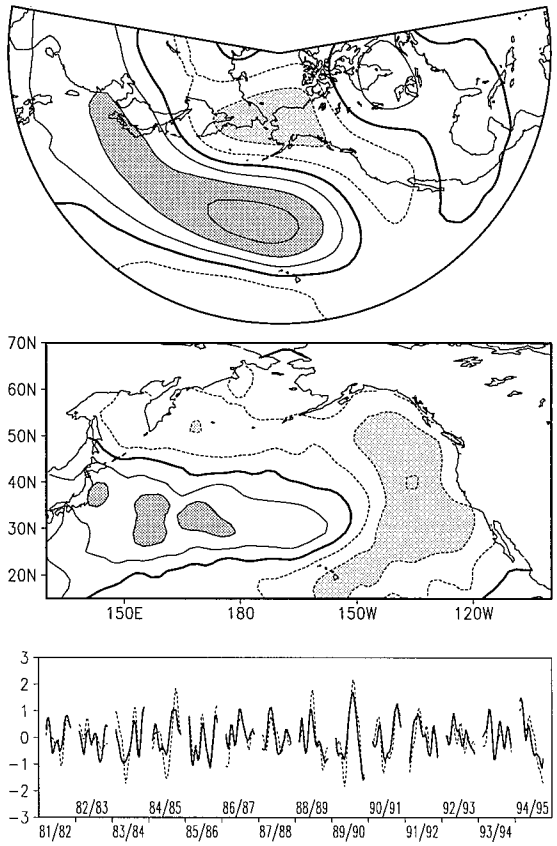

FIG. 13. (a) Heterogeneous correlation patterns for the leading Pacific wintertime SVD mode between 500-mb height (top) and SST tendency (middle; defined as the change in SST from week −2 to week +2 relative to the 500-mb height record). Contour interval = 0.2, with negative contours dashed and the zero contour darkened. Dark (light) shading indicates correlations >0.4 (<−0.4). This mode explains 49% of the coupled variability between the two fields. The expansion coefficients (time series) of the two patterns (bottom) are correlated at 0.80.

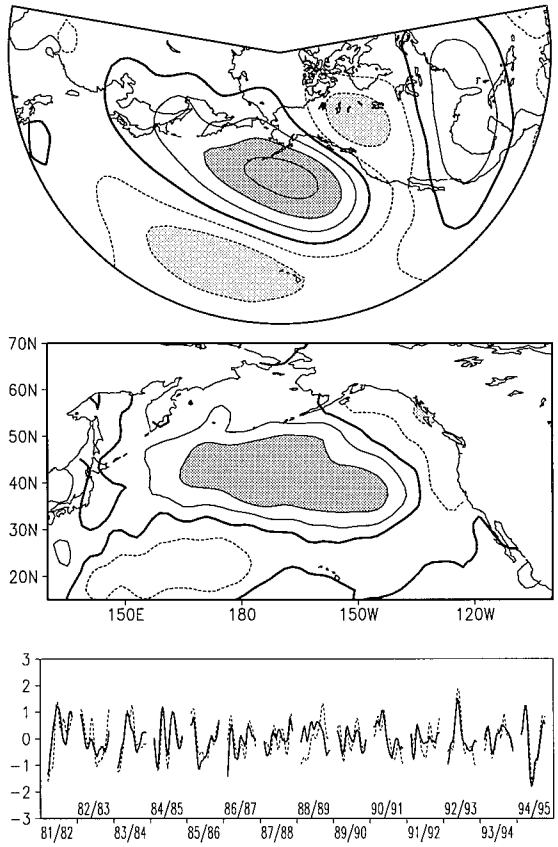

FIG. 14. As in Fig. 13 but for the second Pacific wintertime SVD mode between 500-mb height (top) and SST tendency (middle). This mode explains 32% of the coupled variability and the expansion coefficients of the two patterns (bottom) are correlated at 0.77.

(February–April) as an estimate of the SST tendency and 500-mb heights averaged from December to February. Wallace et al. (1990) found that the spatial patterns of atmosphere–ocean coupling were different for the SST tendency field and the SST field itself. They interpreted their result as evidence for, on the one hand, the atmosphere forcing the ocean (the SST tendency field) and, on the other hand, the ocean forcing the atmosphere (the SST field). While we find no distinction between the patterns of air–sea interaction when we use the SST tendency field versus the SST field, substantial differences between our study and that of Wallace et al. (1990) preclude a direct comparison; for example, Wallace et al. (1990) used a 4-month tendency compared to our 4-week tendency, and Wallace et al. (1990) sampled a much longer period of record (39 yr) compared to our 14-yr period. Further work is needed to resolve the issue of whether on longer timescales (interannual–interdecadal) extratropical SST anomalies can have a significant impact upon the atmospheric circulation.

5. Conclusions

Using weekly data, we showed that the dominant modes of covariability between the atmospheric circulation and SST fields over the North Atlantic and Pacific during winter are characterized by the atmosphere leading the ocean by 2–3 weeks. While this result was anticipated based on previous studies using monthly data, the doubling of the strength of the coupling at 2–3-week lag compared to the contemporaneous relationship was not. We believe the 2–3-week timescale may be a re-

TABLE 7. Time lag in days of the maximum cross correlation between the atmosphere and SST as a function of characteristic timescale, according to the stochastic atmospheric forcing model of Frankignoul and Hasselmann (1977). Here, τ_a refers to the *e*-folding timescale of the atmosphere in days, and τ_{sst} to the *e*-folding timescale of the SST anomalies in months. All time lags indicate the atmosphere leads SST.

		τ_{sst}		
		4	6	8
τ_a	4	11	13	14
	6	14	17	18
	8	17	20	22

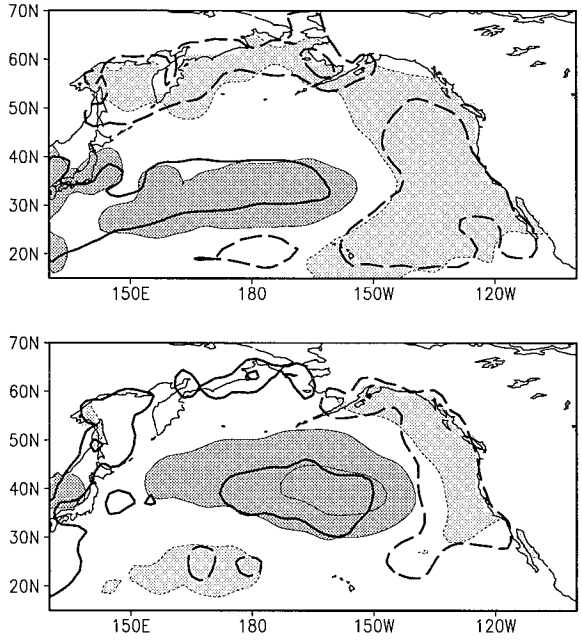

FIG. 15. Observed (shading and thin contours) and heat-flux induced (thick contours) SST tendencies associated with the first (top) and second (bottom) SVD mode in the Pacific. Units are °C per day per unit departure of the SST tendency expansion coefficient. Positive (negative) SST tendency anomalies are indicated by dark shading and solid contours (light shading and dashed contours). Contour levels are −6, −2, 2, and 6.

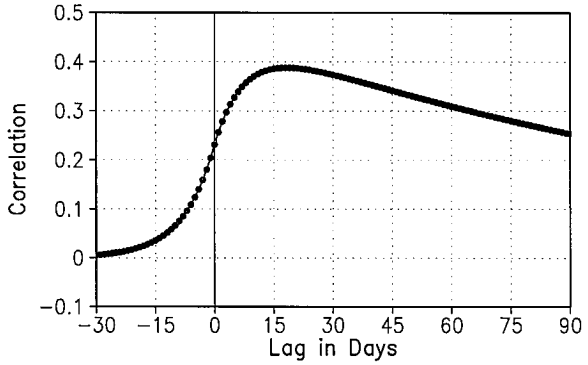

FIG. 16. Theoretical lag cross-correlation curve between the atmosphere and SST, according to the stochastic atmospheric forcing model of Frankignoul and Hasselmann (1977), for *e*-folding timescales of (8 days)$^{-1}$ for the atmospheric forcing and (5 months)$^{-1}$ for SST. Note that the maximum cross correlation occurs at lag +18 days.

flection of high-frequency stochastic forcing by the atmosphere on the ocean mixed layer, in line with the theoretical model of Frankignoul and Hasselmann (1977). Sensible and latent energy fluxes at the sea surface were shown to be an important component of the atmospheric forcing. The close spatial and temporal correspondence between the fluxes and SST tendencies on weekly timescales is a testament to the quality of the datasets.

We have found no evidence for distinct modes of variability indicative of extratropical SST anomalies forcing the atmosphere, a situation that should be reflected in a more symmetric distribution of the lag cross correlations. However, this finding does not preclude the existence of feedback from the ocean to the atmosphere: SST feedback may be contained within the contemporaneous correlations of the dominant modes of covariability. It may also be manifest as increased variability and persistence of certain atmospheric circulation regimes, an aspect not examined here [see Barsugli (1995) and Peng et al. (1995)]. Finally, SST feedback may only be evident on timescales longer than a few years, an issue not adequately addressed in the present study. Further modeling work with realistic high-resolution atmospheric GCMs coupled to an ocean mixed layer model is needed to resolve the issue of the importance of *mutual* interaction in midlatitude atmosphere–ocean variability.

It would be interesting to extend this study to the extratropics in summer, when positive feedbacks between SST and stratiform cloudiness may be important (Klein et al. 1995; R. Ronca and D. Battisti 1997, manuscript submitted to *J. Climate*). It would also be worthwhile to examine the weekly lag associations in the Tropics, where genuine two-way interaction between the atmosphere and ocean is found: does the methodology used here separate the two directions of interaction?

Acknowledgments. We gratefully acknowledge the efforts of Dr. Richard Reynolds in developing the high-quality weekly SST dataset. We thank Drs. Michael Alexander, Joseph Barsugli, Ileana Blade, Shiling Peng, and Professor Mike Wallace for helpful conversations during the course of this work. The comments of the anonymous reviewers helped us to improve the presentation of the results. This research was supported by a grant from the NOAA Office of Global Programs under the auspices of the Atlantic Climate Change Program.

REFERENCES

Alexander, M. A., 1992: Midlatitude atmosphere–ocean interaction during El Nino. Part I: The North Pacific Ocean. *J. Climate,* **5,** 944–958.

Barsugli, J. J., 1995: Idealized models of intrinsic midlatitude atmosphere–ocean interaction. Ph.D. dissertation, University of Washington, 187 pp. [Available on-line from http://www.cdc.noaa.gov/~jjb/thesis.html.]

Battisti, D. S., U. S. Bhatt, and M. A. Alexander, 1995: A modeling study of the interannual variability in the wintertime North Atlantic ocean. *J. Climate,* **8,** 3067–3083.

Bretherton, C. S., C. Smith, and J. M. Wallace, 1992: An intercomparison of methods for finding coupled patterns in climate data. *J. Climate,* **5,** 541–560.

Cayan, D. R., 1992a: Variability of latent and sensible heat fluxes estimated using bulk formulae. *Atmos.–Ocean,* **30,** 1–42.

——, 1992b: Latent and sensible heat flux anomalies over the northern oceans: Driving the sea surface temperature. *J. Phys. Oceanogr.,* **22,** 859–881.

Davis, R. E., 1976: Predictability of sea surface temperature and sea

level pressure anomalies over the North Pacific Ocean. *J. Phys. Oceanogr.*, **6,** 249–266.
Delworth, T. S., 1996: North Atlantic interannual variability in a coupled ocean–atmosphere model. *J. Climate*, **9,** 2356–2375.
Deser, C., and M. L. Blackmon, 1995: On the relationship between tropical and North Pacific SST variations. *J. Climate*, **8,** 1677–1680.
Ferranti, L., F. Molteni, and T. N. Palmer, 1994: Impact of localized tropical and extratropical SST anomalies in ensembles of seasonal GCM integrations. *Quart. J. Roy. Meteor. Soc.*, **120,** 1613–1645.
Frankignoul, C., 1985: Sea surface temperature anomalies, planetary waves, and air–sea feedback in the middle latitudes. *Rev. Geophys.*, **23,** 357–390.
——, and K. Hasselmann, 1977: Stochastic climate models, II, Application to sea surface temperature variability and thermocline variability. *Tellus*, **29,** 284–305.
——, and R. W. Reynolds, 1983: Testing a dynamical model for midlatitude sea surface temperature anomalies. *J. Phys. Oceanogr.*, **13,** 1131–1145.
Hasselmann, K., 1976: Stochastic climate models, I, Theory. *Tellus*, **28,** 473–485.
Held, I. M., 1983: Stationary and quasi-stationary eddies in the extratropical atmosphere: Theory. *Large Scale Dynamical Processes in the Atmosphere*, R. P. Pearce and B. J. Hoskins, Eds., Academic Press, 127–168.
Hense, A., R. G. Hense, H. von Storch, and U. Stahler, 1990: Northern Hemisphere atmospheric response to changes of Atlantic SST on decadal time scales: A GCM experiment. *Climate Dyn.*, **4,** 157–174.
Hoskins, B. J., and D. J. Karoly, 1981: The steady, linear response of a spherical atmosphere to thermal and orographic forcing. *J. Atmos. Sci.*, **38,** 1179–1196.
Klein, S. A., D. L. Hartmann, and J. R. Norris, 1995: Relationships among low-cloud structure, sea surface temperature, and atmospheric circulation in the summertime northeast Pacific. *J. Climate*, **8,** 1140–1155.
Kushnir, Y., 1994: Interdecadal variations in North Atlantic sea surface temperature and associated atmospheric conditions. *J. Climate*, **7,** 141–157.
——, and I. M. Held, 1996: On the equilibrium atmospheric response to North Atlantic SST anomalies. *J. Climate.*, **9,** 1208–1220.
Lanzante, J. R., 1984: A rotated eigenanalysis of the correlation between 700 mb heights and sea surface temperatures in the Pacific and Atlantic. *Mon. Wea. Rev.*, **112,** 2270–2280.
Latif, M., and T. P. Barnett, 1994: Causes of decadal climate variability over the North Pacific and North America. *Science*, **266,** 634–637.
Lau, N.-C., and M. J. Nath, 1994: A modeling study of the relative roles of tropical and extratropical SST anomalies in the variability of the global atmosphere–ocean system. *J. Climate*, **7,** 1184–1207.
Levitus, S., 1982: *Climatological Atlas of the World Ocean.* NOAA Professional Paper No. 13, U.S. Government Printing Office, 173 pp.
Lusksch, U., and H. von Storch, 1992: Modeling the low-frequency sea surface temperature variability in the North Pacific. *J. Climate*, **5,** 893–906.
Miller, A. J., D. R. Cayan, T. P. Barnett, N. E. Graham, and J. M. Oberhuber, 1994: Interdecadal variability of the Pacific Ocean: Model response to observed heat flux and wind stress anomalies. *Climate Dyn.*, **9,** 287–302.
Namias, J., 1959: Recent seasonal interactions between North Pacific waters and the overlying atmospheric circulation. *J. Geophys. Res.*, **64,** 631–646.
——, 1963: Large-scale air–sea interactions over the North Pacific from summer 1962 through the subsequent winter. *J. Geophys. Res.*, **68,** 6171–6186.
——, 1965: Short period climate fluctuations. *Science*, **147,** 696–706.
Newman, M., and P. D. Sardeshmukh, 1995: A caveat concerning singular value decomposition. *J. Climate*, **8,** 352–360.
Palmer, T. N., and Z. Sun, 1985: A modeling and observational study of the relationship between sea surface temperature in the northwest Atlantic and the atmospheric general circulation. *Quart. J. Roy. Meteor. Soc.*, **111,** 947–975.
Peng, S., L. A. Mysak, H. Ritchie, J. Derome, and B. Dugas, 1995: On the difference between early and middle winter atmospheric response to sea surface temperature anomalies in the northwest Atlantic. *J. Climate*, **8,** 137–157.
Reynolds, R. W., 1978: Sea surface temperature in the North Pacific Ocean. *Tellus*, **30,** 97–103.
——, and T. M. Smith, 1995: A high-resolution global sea surface temperature climatology. *J. Climate*, **8,** 1571–1583.
Stommel, H., 1965: *The Gulf Stream: A Physical and Dynamical Description.* University of California Press, 248 pp.
Ting, M., 1991: The stationary wave response to a midlatitude SST anomaly in an idealized GCM. *J. Atmos. Sci.*, **48,** 1249–1275.
Wallace, J. M., and D. S. Gutzler, 1981: Teleconnections in the geopotential height field during the Northern Hemisphere winter. *Mon. Wea. Rev.*, **109,** 784–812.
——, and Q.-R. Jiang, 1987: On the observed structure of the interannual variability of the atmosphere/ocean climate system. *Atmospheric and Oceanic Variability*, H. Cattle, Ed., Roy. Meteor. Soc., 17–43.
——, C. Smith, and Q. Jiang, 1990: Spatial patterns of atmosphere–ocean interaction in the northern winter. *J. Climate*, **3,** 990–998.
——, ——, and C. S. Bretherton, 1992: Singular value decomposition of wintertime sea surface temperature and 500-mb height anomalies. *J. Climate*, **5,** 561–576.